FRONTIERS OF PHYSICS

RESEARCH ARTICLE
Volume 17 / Issue 5 / 52505 / 2022

A driven three-dimensional electric lattice for polar molecules

Hengjiao Guo, Yabing Ji, Qing Liu, Tao Yang, Shunyong Hou†, Jianping Yin‡

State Key Laboratory of Precision Spectroscopy, East China Normal University, Shanghai 200062, China
Corresponding authors. E-mail: †syhou@lps.ecnu.edu.cn, ‡jpyin@phy.ecnu.edu.cn
Received March 24, 2022; accepted May 9, 2022

ABSTRACT

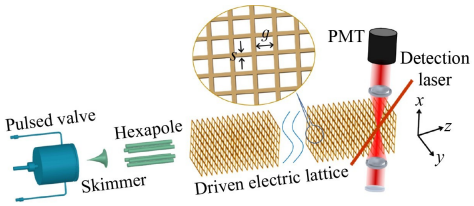

Three-dimensional (3D) driven optical lattices have attained great attention for their wide applications in the quest to engineer new and exotic quantum phases. Here we propose a 3D driven electric lattice (3D-DEL) for cold polar molecules as a natural extension. Our 3D electric lattice is composed of a series of thin metal plates in which two-dimensional square hole arrays are distributed. When suitable modulated voltages are applied to these metal plates, a 3D potential well array for polar molecules can be generated and can move smoothly back and forth in the lattice. Thus, it can drive cold polar molecules confined in the 3D electric lattice. Theoretical analyses and trajectory calculations using two types of molecules, ND_3 and PbF, are performed to justify the possibility of our scheme. The 3D-DEL offers a platform for investigating cold molecules in periodic driven potentials, such as quantum computing science, quantum information processing, and some other possible applications amenable to the driven optical lattices.

Keywords 3D driven electric lattice, cold polar molecules

1 Introduction

With the development of laser cooling and trapping techniques [1–5], the periodic optical lattices based on the interference of intersecting laser beams [6] have become ideal tools for studying fundamental physics experiments and quantum information processing, such as the simulations of condensed matter phenomena [7], quantum gases microscopes [8], high precision atomic clocks [9], and quantum gates for quantum information [10, 11]. Furthermore, periodically driven quantum systems can produce many fascinating physics and phenomena inaccessible to their static counterparts [12–15]. Therefore, the optical lattice subject to a time-periodic driving potential becomes an important tool for realizing quantum simulations and manipulating ultracold atomic quantum gases [16]. By confining atoms or molecules to such an optical lattice potential, many meaningful studies have been realized, such as the coherent control of the single-particle tunneling amplitude in periodically shaken lattice [17], the implementation of kinematic frustration [18, 19], and the study of the kinetics of phase transitions [20, 21].

Compared to the rapid progress in the driven optical lattice, little work has been done on the electric lattice. Here we propose a three-dimensional driven electric lattice (3D-DEL) for polar molecules, analogous to the driven optical lattice for cold atoms. The polar molecules, with their rich structure of internal states and tunable long-range electric dipole–dipole interactions, play an essential role in the studies of quantum simulation of phases of matter [22–26], precision measurements [27–29], cold chemistry [30–32], cold collisions [33], and high-fidelity quantum information processing [34–37]. Moreover, our 3D-DEL can generate periodic electrostatic microtraps in the lattice by applying suitable voltages. Besides, the 3D electric lattice can also slow down supersonic molecular beams to a standstill and trap them in the lattice. In a word, thus 3D electric lattice can offer a variety of control methods for cold

Higher Education Press

https://doi.org/10.1007/s11467-022-1174-1

polar molecules.

In the following sections, we will first present the design of the 3D-DEL. Following that, theoretical analyses and trajectory calculations using two types of molecules, ND_3 and PbF, are given to justify the possibility of our scheme. The end is the conclusions and outlook.

2 Design

Figure 1 shows our three-dimensional driven electric lattice (3D-DEL) schematic diagram in a cold molecular experiment. A beam of polar molecules is released into a vacuum and then is loaded into the 3D-DEL. The manipulated molecules can be detected by laser-induced fluorescence at the end of the lattice.

The 3D-DEL is composed of a series of thin metal plates that are patterned with a 2D periodical square hole array. The thickness of each plate is c, and the distance between the centers of the adjacent plates is d. The detailed view of the plate is shown in Fig. 1, where the length of a square hole in the plate is s and the width of the metal frame between two neighboring square holes is g. By applying appropriate voltages on these metal plates, a moving 3D electric potential array can be formed among the 3D-DEL.

3 Principle of operation

The potential on each individual electrode plate can be expressed as

$$V_n(t) = V_0 \sin\left(\varphi(t) + \frac{2\pi n}{N}\right), \tag{1}$$

with the waveform amplitude being V_0 and the time-dependent phase offset being $\varphi(t)$. N is the number of electrodes in one longitudinal periodicity, and thus the longitudinal periodicity of the 3D-DEL is $L_1 = Nd$. The voltage is applied in a manner similar to that of the traveling wave Stark decelerator [38]. These voltages create two electric field minima in one longitudinal periodicity. At the same time, according to the periodic structure of the lattice in the transverse directions, a periodic electric field minimum can also be generated by applying the above voltages. The length of the transverse periodicity is $L_2 = s + g$. Transverse and longitudinal minima represent the formation of a three-dimensional trap array for polar molecules. By modulating these voltages sinusoidally, the minima of the longitudinal electric field can be moved along the lattice. The time-dependent of the phase offset is given by

$$\varphi(t) = 2\pi \int_0^t \omega(\tau)\, \mathrm{d}\tau, \tag{2}$$

where $\omega(\tau)$ is the modulation frequency and is directly linked to the longitudinal trap velocity expressed as $v_z = L_1\omega(\tau)$. After applying the above voltages, the electric potential $\phi(x, y, z)$ in the 3D-DEL can be obtained by

$$\begin{aligned}\phi(x,y,z) = \sum_{m,n,l}^{\infty} C_{mnl} &[\cos(mk_x x) + \sin(mk_x x)] \\ &\times [\cos(nk_y y) + \sin(nk_y y)] \\ &\times [\cos(lk_z z) + \sin(lk_z z)],\end{aligned} \tag{3}$$

where $k_x = k_y = 2\pi/L_2$, $k_z = 2\pi/L_1$. In the following discussions, the geometrical parameters combination of the lattice are set as follows: $c = g = 10$ μm, $d = 40$ μm, and $s = 50$ μm. It should be noted that the geometric size of the electrode plate can be scaled up or down as needed. To create the suitable potential for ND_3 molecules in the $|J, MK\rangle = |1, -1\rangle$ state, V_0 is set to 100 V, and N is set to 8. When m, n, l are integers from 0 to 2, the coefficients C_{mnl} can be determined by comparing each Fourier component with Eq. (3), using a method similar to the reference [39]. Once the electric potential is constrained, the electric field strength is given by

$$|\boldsymbol{E}| = \sqrt{\left(\frac{\partial\phi}{\partial x}\right)^2 + \left(\frac{\partial\phi}{\partial y}\right)^2 + \left(\frac{\partial\phi}{\partial z}\right)^2}. \tag{4}$$

Figure 2(a) illustrates four snapshots of the Stark potential along the z-axis when moving through one stage of the lattice. In case (1), the two potential minima are just in the electrodes located at 0 μm and 160 μm, respectively. In cases (2)–(5), with the linear increase of $\varphi(t)$, the minima of potential are shifting along the z-axis continuously. The offset in case (5) is 40 μm compared to the case (1), which corresponds to a shift of $\pi/4$ for the phase of the applied voltages. In each case, the maximum value of the longitudinal electric field remains constant at 18 kV/cm. Figure 2(b) shows the electric field distributions in the transverse (x–y planes) through the minima of the lattice sites, which are right between two neighboring electrode plants. For ND_3 molecules, the maximum value of the transverse electric field is 3 kV/cm, corresponding to a potential trap depth of 27.5 mK.

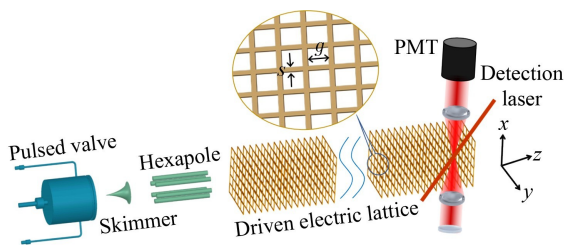

Fig. 1 Schematic view of the 3D-DEL in a cold molecular experiment. A molecular beam is generated by a pulse valve, and then is coupled into the 3D-DEL by a hexapole. After being manipulated by the 3D-DEL, the molecules can be detected by laser-induced fluorescence.

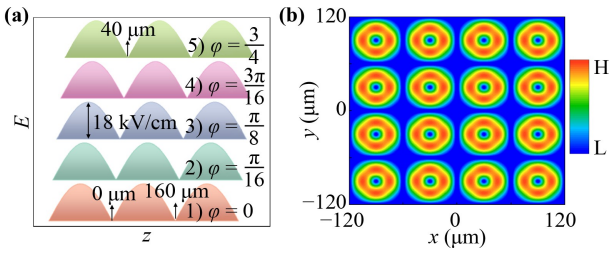

Fig. 2 **(a)** The operation principle of the electric fields in the 3D-driven electric lattice. **(b)** The electric field distribution of the 3D lattice in the transverse (x–y plane) directions through the electric field minima of the lattice sites.

4 Theoretical analysis and trajectory calculations

To justify the performance of our 3D-DEL for polar molecules, theoretical analysis and 3D numerical calculations are carried out with ND_3 molecules. ND_3 is a kind of symmetric top molecule with a pyramidal structure. In zero electric field, the $|J,K\rangle = |1,1\rangle$ level of ND_3 is split due to tunneling in a symmetric and in an antisymmetric component. Upon applying an electric field, the symmetric and the antisymmetric components interact and repel each other, leading to four levels, as shown in Fig. 3. Throughout the following simulations, molecules in the $|J,MK\rangle = |1,-1\rangle$ state is used, which is the only low-field-seeking state populated in the molecular beam.

For ND_3 molecule, the stark energy of $|J,K\rangle = |1,1\rangle$ varying with the magnitude of the external electric field can be obtained by [40]

$$W(|\boldsymbol{E}|) = \pm\sqrt{\left(\frac{W_{inv}}{2}\right)^2 + \left(\mu|\boldsymbol{E}|\frac{MK}{J(J+1)}\right)^2} - \frac{W_{inv}}{2}, \tag{5}$$

where W_{inv} is the zero-field inversion splitting ($0.053\ \mathrm{cm}^{-1}$ for ND_3), μ is the permanent electric dipole moment (1.5 Debye for ND_3), and M,K are the projections of the

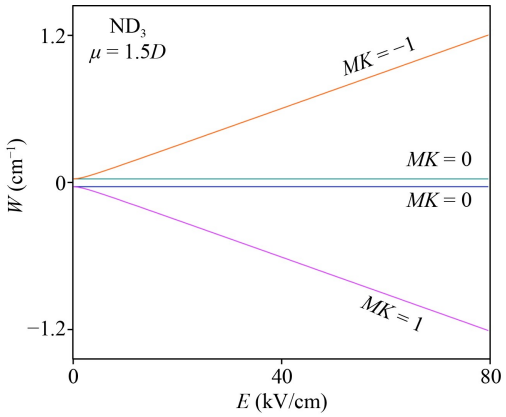

Fig. 3 Stark shift of the $|J,K\rangle = |1,1\rangle$ level of ND_3 ammonia molecules in an electric field of up to 80 kV/cm.

total angular momentum J on the electric field $|\boldsymbol{E}|$ and along the symmetry axis, respectively. As can be seen from Eq. (5), the Stark shift is quadratic for low electric field strengths and becomes linear when the Stark interaction becomes large relative to the zero-field splitting [41]. After obtaining the stark potential, the force between the ND_3 molecules and the fields can be derived from the following expression [39]:

$$\begin{pmatrix} F_x \\ F_y \\ F_z \end{pmatrix} = -\left(\frac{1}{|\boldsymbol{E}|}\frac{\mathrm{d}W}{\mathrm{d}|\boldsymbol{E}|}\right)\begin{pmatrix} \frac{\partial^2\phi}{\partial x^2} & \frac{\partial^2\phi}{\partial x\partial y} & \frac{\partial^2\phi}{\partial x\partial z} \\ \frac{\partial^2\phi}{\partial x\partial y} & \frac{\partial^2\phi}{\partial y^2} & \frac{\partial^2\phi}{\partial y\partial z} \\ \frac{\partial^2\phi}{\partial x\partial z} & \frac{\partial^2\phi}{\partial y\partial z} & \frac{\partial^2\phi}{\partial z^2} \end{pmatrix}\begin{pmatrix} \frac{\partial\phi}{\partial x} \\ \frac{\partial\phi}{\partial y} \\ \frac{\partial\phi}{\partial z} \end{pmatrix}. \tag{6}$$

In our 3D-DEL, the longitudinal motion of the ND_3 molecule relative to the moving potential well center can be given by

$$m\frac{\mathrm{d}^2\Delta z}{\mathrm{d}t^2} + ma - \overline{F}(\Delta z) = 0, \tag{7}$$

where Δz is the instantaneous longitudinal position difference between the molecule and the potential well center, m is the mass of the ND_3 molecule, and a is the acceleration of the potential well. $\overline{F}(\Delta z)$ is the average force experienced by molecules in the potential well over one period, which can be obtained from Eqs. (3)–(6). For the ND_3 molecule, the phase acceptance of an individual trap of the electric lattice along the longitudinal direction can be obtained from Eq. (7). By integrating Eq. (7), the phase-stability diagram in the longitudinal direction with the acceleration of the lattice being zero is shown in Fig. 4(a). The molecules are phase-stable when they are in the area inside the separatrix. In contrast, those beyond the separatrix will be lost because their total energy is larger than the effective potential. We also calculate the effective potential for ND_3 molecule in the lattice when the acceleration of the lattice is zero. The depth of the potential well of our 3D-DEL is about 0.43 K when $a = 0\ \mu\mathrm{m}\cdot\mu\mathrm{s}^{-2}$, as shown in Fig. 4(b). For transverse direction, the motion of the molecules in the moving trap can be written as

$$m\frac{\mathrm{d}^2x,y}{\mathrm{d}t^2} - \overline{F}_{x,y} = 0, \tag{8}$$

where $\overline{F}_{x,y}$ is the average transverse force experienced by molecules and is written as $\overline{F}_{x,y} = \int_0^{L_1}\frac{F_{x,y}(\varphi(t),z)}{L_1}\mathrm{d}z$.

Our simulation covers the whole dynamic process, including loading, deceleration, and detection. In the simulation, the losses caused by background collision and surface-induced heating are ignored as current vacuum and cooling technology significantly reduce these losses [42]. Because of the non-zero pseudo potential well centers in the driven lattice, the nonadiabatic tran-

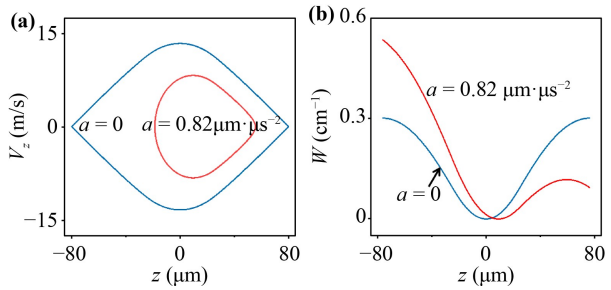

Fig. 4 The phase space separatrices **(a)** and effective potential wells **(b)** for the ND_3 molecules in the moving electric lattice along the longitudinal direction, with the acceleration of the lattice being $a = 0$ μm·μs^{-2} and $a = 0.82$ μm·μs^{-2}.

sition loss can also not be considered in our calculation [43]. The six-dimensional emittance of the initial molecular beam in our simulation is set to be $(\Delta z \times \Delta \nu_z) \times (\Delta x \times \Delta \nu_x) \times (\Delta y \times \Delta \nu_y) = (800\ \mu\text{m} \times 15\ \text{m/s}) \times (500\ \mu\text{m} \times 5\ \text{m/s}) \times (500\ \mu\text{m} \times 5\ \text{m/s})$, where the position and velocity spread are flat in all directions. The incident beam contains 5×10^6 molecules with an initial distribution centered at $z = 0$ μm, $v_z = 330$ m/s, $y = 30$ μm, $v_y = 0$ m/s and $x = 30$ μm, $v_x = 0$ m/s. The above parameters of the tailored molecular beam are chosen by referring to the related experimental parameters [44]. In the calculation, the transverse dimension of the lattice is set to 9 mm × 9 mm, and the longitudinal dimension is about 6.7 cm. The waveform amplitude V_0 applied on the electrodes is set to 100 V.

In the simulation, we employ a so-called "synchronous molecule" to create the time sequence of operations. The synchronous molecule is virtual and is always in sync with operations of the external fields. The beam of ND_3 molecule first freely flies at a distance of 10 mm and then is loaded into the 3D-DEL along the longitudinal direction. To match the central velocity (330 m/s) of the incident molecular beam, the initial frequency of the modulated voltages applied on the electrode plates of the lattice is set to 6.48 MHz. Then the frequency of the modulated voltages is continuously chirped from 6.48 MHz to 0 Hz in about 0.42 ms, resulting in acceleration up to 0.82 μm·μs^{-2}. We calculated the phase space separatrix and effective potential well for the ND_3 molecules in the lattice when the acceleration is 0.82 μm·μs^{-2} and the results are shown in Fig. 4. It is clear that compared to the case of zero acceleration, the separatrix gets smaller, and the depth of the potential becomes shallower. The center of the potential well also shifts forward slightly.

The results of the trajectory calculation of the decelerated ND_3 molecules are shown in Fig. 5. With a deceleration strength of 0.82 μm·μs^{-2}, a beam of ND_3 molecules with an initial velocity of 330 m/s can be decelerated to a standstill by our 3D-DEL. Figure 5(a) indicates the transverse spatial distribution of the molecular packets at the end of the lattice with a forward velocity being close to zero. Fig. 5(b) shows the calculated result of the ND_3 molecule distribution in the longitudinal phase space when a=0.82 μm·μs^{-2}, together with the corresponding longitudinal acceptance of the lattice. These enriching distribution for molecules in both transverse and longitudinal phase space illustrates the stability of the deceleration process in the lattice.

It has been known for a long time that heavy molecules (roughly defined as mass >100 amu) are of particular interest in the test of fundamental physics, such as the measurements of electric dipole moment (EDM) of the electron [45] and tests of parity violation in nuclei [46] and chiral molecules [47]. However, it is usually more challenging to tame heavy polar molecules because they have more kinetic energy for a given velocity, and their Stark curve of the rotational energy levels easily turns down at high electric fields. To confirm the performance of our proposed 3D-DEL in manipulating heavy polar molecules, PbF molecule is used here as a tester. We chose the PbF molecule as the prototype molecule for our simulations because it is predicted to be a sensitive probe for measurement of e-EDM [48], and because it has a reasonable dipole moment (3.5 Debye), rotational moment, and corresponding Stark shift. The Stark shift of the PbF of the lowest rotational levels in the vibronic ground state is shown in Fig. 6(a). The $(N, N_M) = (2, 0)$ is selected for the following studies, where N is the rotational quantum number and N_M is the projection of N on the electric field axis. The maximum electric field along the longitudinal direction of the lattice is 54 kV/cm under V_0 being set to 300 V, where PbF molecule in the state (2,0) is still a weak-field-seeker. To decelerate PbF molecules from a supersonic speed to zero, the number of slowing stages is increased to 6640, resulting in the total length of the lattice up to about 26 cm, which is still greatly shorter than the currently used decelerator for heavy polar molecules [49]. All other lattice parameters used here are identical to those of the above sections. With the acceleration of the lattice being 0.2 μm·μs^{-2}, the packet of PbF molecules are lowered

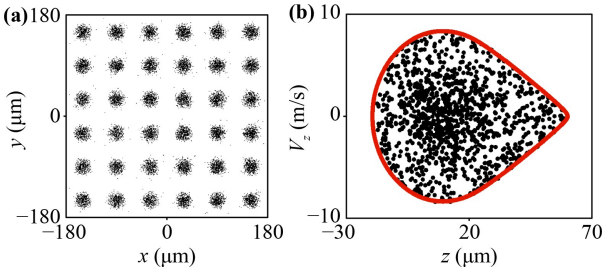

Fig. 5 **(a)** The 2D view of the molecular distribution at the end of the lattice with a longitudinal velocity being close to zero in the x−y plane. **(b)** The longitudinal separatrix for the lattice with the acceleration of 0.82 μm·μs^{-2} (solid red line), together with the decelerated ND_3 molecules in the lattice (black dots).

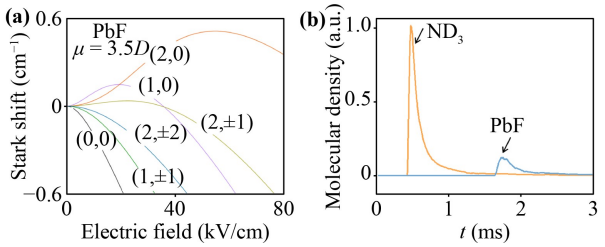

Fig. 6 **(a)** The Stark shift of PbF in low-lying rotational states (N, N_M), where N is the rotational number and N_M is the projection of N on the electric field axis. **(b)** Simulated time-of-flight profiles for ND_3 and PbF molecules.

from 330 m/s to near a standstill, as shown in Fig. 6(a). For comparison, the TOF (time of flight) profile for ND_3 molecules are also plotted in Fig. 6(b). The result shows that our 3D-DEL can effectively slow down heavy polar molecules in low-field-seeking states, benefited from its stable 3D confinement in the slowing process. This lattice may find applications in the miniaturization of heavy molecular control instruments.

At the end of the 3D lattice, the moving potentials are brought to a standstill, and the molecules in the traps can be stably confined in the lattice, where further molecular experiments can be performed. The time dependence of ND_3 and PbF molecules in the stationary 3D lattice are shown in Fig. 7. It is clear that both the ND_3 molecules and PbF molecules can be stably confined in the 3D-DEL. The polar molecules trapped in the lattice promise a variety of applications ranging from cold collisions to precision measurement and some other possible applications amenable to magnetic or optical lattices.

The results of the above simulations have confirmed that the 3D-DEL can effectively manipulate both light and heavy polar molecules, including deceleration and trapping them. Furthermore, the 3D potential wells can be moved back and forth by varying the voltages on the lattice. This operation is similar to driven optical [50] or

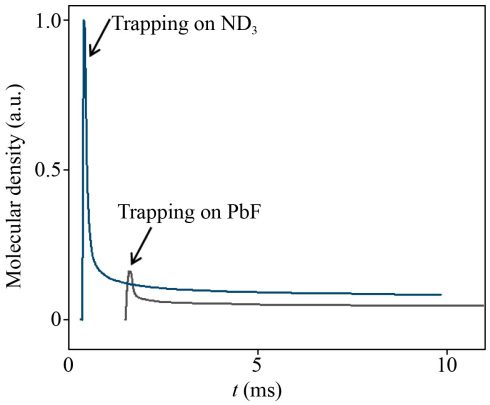

Fig. 7 Time dependence of molecular density of trapping process for ND_3 molecules and PbF molecules respectively in the 3D-DEL.

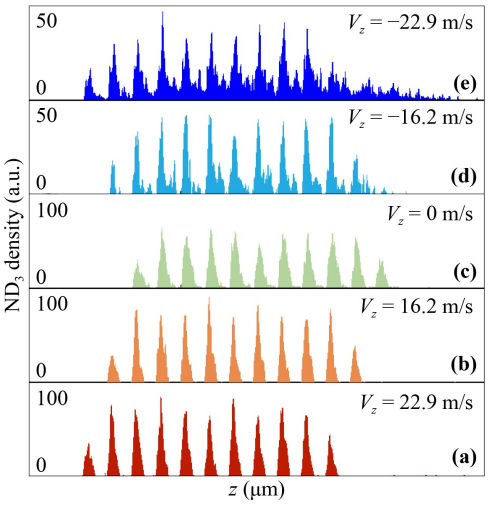

Fig. 8 Shuttling back and forth arrays of ND_3 molecules in our 3D-DEL. The velocities of the lattice are indicated in each case.

magnetic lattices [51], that is why we call our lattice a driven lattice. To justify the performance of our 3D-DEL, trajectory calculations for ND_3 molecules are performed with the same parameters used in previous sections. A ND_3 molecular beam loaded into the potential well can be decelerated to rest and then accelerated in the opposite direction with the same acceleration. Some snapshots of this deceleration process are depicted in Figs. 8 (a)–(c), where ND_3 molecular packets are gradually stopped near the end of the lattice. Following that, the molecular packets are then shifted back with the same acceleration. As shown in Figs. 8(c)–(e), the packets are accelerated from a standstill to 22.9 m/s. That is to say, they are moving in the opposite direction from where they started. In our simulations, the detection laser is perpendicular to the molecular beam axis and each peak in Fig. 8 represents an 11×11 array. The spatial interval between the adjacent snapshots in Fig. 8 is 160 μm.

5 Conclusions

We have proposed a 3D-driven electric lattice for polar molecules, which is composed of arrays of equidistant mental plates with sine-modulated voltages. By chirping the frequency of the voltage applied to the electrodes, the three-dimensional electrostatic micro traps can move back and forth smoothly through the lattice. These microtraps allow polar molecules to be decelerated and trapped in the lattice. Two types of sample molecules, ND_3 (in the $|J, MK\rangle = |1, -1\rangle$ state) and PbF (in the $|N, N_M\rangle = |2, 0\rangle$ state) are used in our numerical calculations to justify the possibility of our scheme. If combined with other cooling methods, such as adiabatic cooling [52], Sisyphus cooling [53], or evaporative cooling [54], the 3D-DEL can produce arrays of ultracold molecular

samples. In addition, since the potential wells in the lattice are true 3D traps for polar molecules, the 3D-DEL allows confining different molecular beams in different parts of the lattice simultaneously, which may provide many intriguing applications in cold molecule studies. Due to its rich operation means, the 3D-DEL, might have potential applications in quantum simulation studies, similar to that of the driven optical lattices for ultracold atoms [55].

Acknowledgements This work was supported by the National Natural Science Foundation of China (Grant Nos. 11834003, 91536218, and 11874151), the Fundamental Research Funds for the Central Universities, the Program for Professor of Special Appointment (Eastern Scholar) at Shanghai Institutions of Higher Learning, and the Young Top-Notch Talent Support Program of Shanghai.

References

1. S. Chu, Nobel Lecture: The manipulation of neutral particles, *Rev. Mod. Phys.* 70(3), 685 (1998)
2. C. N. Cohen-Tannoudji, Nobel Lecture: Manipulating atoms with photons, *Rev. Mod. Phys.* 70(3), 707 (1998)
3. W. D. Phillips, Nobel Lecture: Laser cooling and trapping of neutral atoms, *Rev. Mod. Phys.* 70(3), 721 (1998)
4. Q. Liang, T. Chen, W. H. Bu, Y. H. Zhang, and B. Yan, Laser cooling with adiabatic passage for type-II transitions, *Front. Phys.* 16(3), 32501 (2021)
5. K. Yan, R. Gu, D. Wu, J. Wei, Y. Xia, and J. Yin, Simulation of EOM-based frequency-chirped laser slowing of MgF radicals, *Front. Phys.* 17(4), 42502 (2022)
6. I. Bloch, Ultracold quantum gases in optical lattices, *Nat. Phys.* 1(1), 23 (2005)
7. I. Bloch, J. Dalibard, and W. Zwerger, Many-body physics with ultracold gases, *Rev. Mod. Phys.* 80(3), 885 (2008)
8. W. S. Bakr, J. I. Gillen, A. Peng, S. Fölling, and M. Greiner, A quantum gas microscope for detecting single atoms in a Hubbard-regime optical lattice, *Nature* 462(7269), 74 (2009)
9. M. Takamoto, F. L. Hong, R. Higashi, and H. Katori, An optical lattice clock, *Nature* 435(7040), 321 (2005)
10. T. Calarco, E. A. Hinds, D. Jaksch, J. Schmiedmayer, J. I. Cirac, and P. Zoller, Quantum gates with neutral atoms: Controlling collisional interactions in time-dependent traps, *Phys. Rev. A* 61(2), 022304 (2000)
11. C. Monroe, Quantum information processing with atoms and photons, *Nature* 416(6877), 238 (2002)
12. M. S. Rudner, N. H. Lindner, E. Berg, and M. Levin, Anomalous edge states and the bulk-edge correspondence for periodically driven two-dimensional systems, *Phys. Rev. X* 3(3), 031005 (2013)
13. V. Bastidas, C. Emary, B. Regler, and T. Brandes, Nonequilibrium quantum phase transitions in the Dicke model, *Phys. Rev. Lett.* 108(4), 043003 (2012)
14. S. Choi, D. A. Abanin, and M. D. Lukin, Dynamically induced many-body localization, *Phys. Rev. B* 97(10), 100301 (2018)
15. D. S. Bhakuni, R. Nehra, and A. Sharma, Drive-induced many-body localization and coherent destruction of Stark many-body localization, *Phys. Rev. B* 102(2), 024201 (2020)
16. A. Eckardt, Colloquium: Atomic quantum gases in periodically driven optical lattices, *Rev. Mod. Phys.* 89(1), 011004 (2017)
17. H. Lignier, C. Sias, D. Ciampini, Y. Singh, A. Zenesini, O. Morsch, and E. Arimondo, Dynamical control of matter-wave tunneling in periodic potentials, *Phys. Rev. Lett.* 99(22), 220403 (2007)
18. A. Eckardt, M. Holthaus, H. Lignier, A. Zenesini, D. Ciampini, O. Morsch, and E. Arimondo, Exploring dynamic localization with a Bose−Einstein condensate, *Phys. Rev. A* 79(1), 013611 (2009)
19. C. E. Creffield, F. Sols, D. Ciampini, O. Morsch, and E. Arimondo, Expansion of matter waves in static and driven periodic potentials, *Phys. Rev. A* 82(3), 035601 (2010)
20. L. W. Clark, L. Feng, and C. Chin, Universal space-time scaling symmetry in the dynamics of bosons across a quantum phase transition, *Science* 354(6312), 606 (2016)
21. L. Feng, L. W. Clark, A. Gaj, and C. Chin, Coherent inflationary dynamics for Bose–Einstein condensates crossing a quantum critical point, *Nat. Phys.* 14(3), 269 (2018)
22. A. V. Gorshkov, S. R. Manmana, G. Chen, E. Demler, M. D. Lukin, and A. M. Rey, Quantum magnetism with polar alkali-metal dimers, *Phys. Rev. A* 84(3), 033619 (2011)
23. J. Levinsen, N. R. Cooper, and G. V. Shlyapnikov, Topological $p_x+ ip_y$ superfluid phase of fermionic polar molecules, *Phys. Rev. A* 84(1), 013603 (2011)
24. M. A. Baranov, M. Dalmonte, G. Pupillo, and P. Zoller, Condensed matter theory of dipolar quantum gases, *Chem. Rev.* 112(9), 5012 (2012)
25. M. Wall, K. Hazzard, and A. M. Rey, *Quantum magnetism with ultracold molecules*, in: From Atomic to Mesoscale: The Role of Quantum Coherence in Systems of Various Complexities, World Scientific, 2015, page 3
26. N. Y. Yao, M. P. Zaletel, D. M. Stamper-Kurn, and A. Vishwanath, A quantum dipolar spin liquid, *Nat. Phys.* 14(4), 405 (2018)
27. I. Kozyryev, and N. R. Hutzler, Precision measurement of time-reversal symmetry violation with laser-cooled polyatomic molecules, *Phys. Rev. Lett.* 119(13), 133002 (2017)
28. S. Kondov, C. H. Lee, K. Leung, C. Liedl, I. Majewska, R. Moszynski, and T. Zelevinsky, Molecular lattice clock with long vibrational coherence, *Nat. Phys.* 15(11), 1118 (2019)
29. J. Lim, J. Almond, M. Trigatzis, J. Devlin, N. Fitch, B. Sauer, M. Tarbutt, and E. Hinds, Laser cooled YbF molecules for measuring the electron's electric dipole moment, *Phys. Rev. Lett.* 120(12), 123201 (2018)
30. S. Ospelkaus, K. K. Ni, D. Wang, M. De Miranda, B. Neyenhuis, G. Quéméner, P. Julienne, J. Bohn, D. Jin, and J. Ye, Quantum-state controlled chemical reactions of ultracold potassium-rubidium molecules, *Science* 327(5967), 853 (2010)

31. A. Klein, Y. Shagam, W. Skomorowski, P. S. Żuchowski, M. Pawlak, L. Janssen, N. Moiseyev, S. Y. van de Meerakker, A. van der Avoird, C. P. Koch, and E. Narevicius, Directly probing anisotropy in atom–molecule collisions through quantum scattering resonances, *Nat. Phys.* 13(1), 35 (2017)
32. M. G. Hu, Y. Liu, D. D. Grimes, Y. W. Lin, A. H. Gheorghe, R. Vexiau, N. Bouloufa-Maafa, O. Dulieu, T. Rosenband, and K. K. Ni, Direct observation of bimolecular reactions of ultracold KRb molecules, *Science* 366(6469), 1111 (2019)
33. Y. Liu and L. Luo, Molecular collisions: From near-cold to ultra-cold, *Front. Phys.* 16(4), 42300 (2021)
34. D. DeMille, Quantum computation with trapped polar molecules, *Phys. Rev. Lett.* 88(6), 067901 (2002)
35. K. K. Ni, T. Rosenband, and D. D. Grimes, Dipolar exchange quantum logic gate with polar molecules, *Chem. Sci.* 9(33), 6830 (2018)
36. E. R. Hudson and W. C. Campbell, Dipolar quantum logic for freely rotating trapped molecular ions, *Phys. Rev. A* 98(4), 040302 (2018)
37. V. V. Albert, J. P. Covey, and J. Preskill, Robust encoding of a qubit in a molecule, *Phys. Rev. X* 10(3), 031050 (2020)
38. A. Osterwalder, S. A. Meek, G. Hammer, H. Haak, and G. Meijer, Deceleration of neutral molecules in macroscopic traveling traps, *Phys. Rev. A* 81(5), 051401 (2010)
39. S. A. Meek, S. A. Meek, Ph. D. thesis, Freie Universität, 2010
40. S. Y. van de Meerakker, H. L. Bethlem, N. Vanhaecke, and G. Meijer, Manipulation and control of molecular beams, *Chem. Rev.* 112(9), 4828 (2012)
41. H. L. Bethlem, F. M. Crompvoets, R. T. Jongma, S. Y. van de Meerakker, and G. Meijer, Deceleration and trapping of ammonia using time-varying electric fields, *Phys. Rev. A* 65(5), 053416 (2002)
42. S. Y. Buhmann, M. Tarbutt, S. Scheel, and E. Hinds, Surface-induced heating of cold polar molecules, *Phys. Rev. A* 78(5), 052901 (2008)
43. S. A. Meek, G. Santambrogio, B. G. Sartakov, H. Conrad, and G. Meijer, Suppression of nonadiabatic losses of molecules from chip-based microtraps, *Phys. Rev. A* 83(3), 033413 (2011)
44. F. M. H. Crompvoets, R. T. Jongma, H. L. Bethlem, A. J. A. van Roij, and G. Meijer, Longitudinal focusing and cooling of a molecular beam, *Phys. Rev. Lett.* 89(9), 093004 (2002)
45. J. J. Hudson, D. M. Kara, I. Smallman, B. E. Sauer, M. R. Tarbutt, and E. A. Hinds, Improved measurement of the shape of the electron, *Nature* 473(7348), 493 (2011)
46. D. DeMille, S. B. Cahn, D. Murphree, D. A. Rahmlow, and M. G. Kozlov, Using molecules to measure nuclear spin-dependent parity violation, *Phys. Rev. Lett.* 100(2), 023003 (2008)
47. B. Darquié, C. Stoeffler, A. Shelkovnikov, C. Daussy, A. Amy-Klein, C. Chardonnet, S. Zrig, L. Guy, J. Crassous, P. Soulard, P. Asselin, T. R. Huet, P. Schwerdtfeger, R. Bast, and T. Saue, Progress toward the first observation of parity violation in chiral molecules by high-resolution laser spectroscopy, *Chirality* 22(10), 870 (2010)
48. K. Baklanov, A. Petrov, A. Titov, and M. Kozlov, Progress toward the electron electric-dipole-moment search: Theoretical study of the PbF molecule, *Phys. Rev. A* 82(6), 060501 (2010)
49. P. Aggarwal, Y. Yin, K. Esajas, H. Bethlem, A. Boeschoten, A. Borschevsky, S. Hoekstra, K. Jungmann, V. Marshall, T. Meijknecht, M. C. Mooij, R. G. E. Timmermans, A. Touwen, W. Ubachs, and L. Willmann, Deceleration and trapping of SrF molecules, *Phys. Rev. Lett.* 127(17), 173201 (2021)
50. J. Struck, C. Ölschläger, M. Weinberg, P. Hauke, J. Simonet, A. Eckardt, M. Lewenstein, K. Sengstock, and P. Windpassinger, Tunable gauge potential for neutral and spinless particles in driven optical lattices, *Phys. Rev. Lett.* 108(22), 225304 (2012)
51. A. Soba, P. Tierno, T. M. Fischer, and F. Saguès, Dynamics of a paramagnetic colloidal particle driven on a magnetic-bubble lattice, *Phys. Rev. E* 77(6), 060401 (2008)
52. B. G. Englert, M. Mielenz, C. Sommer, J. Bayerl, M. Motsch, P. W. Pinkse, G. Rempe, and M. Zeppenfeld, Storage and adiabatic cooling of polar molecules in a microstructured trap, *Phys. Rev. Lett.* 107(26), 263003 (2011)
53. M. Zeppenfeld, B. G. Englert, R. Glöckner, A. Prehn, M. Mielenz, C. Sommer, L. D. van Buuren, M. Motsch, and G. Rempe, Sisyphus cooling of electrically trapped polyatomic molecules, *Nature* 491(7425), 570 (2012)
54. J. Märkle, A. Allen, P. Federsel, B. Jetter, A. Günther, J. Fortágh, N. Proukakis, and T. Judd, Evaporative cooling of cold atoms at surfaces, *Phys. Rev. A* 90(2), 023614 (2014)
55. F. Schäfer, T. Fukuhara, S. Sugawa, Y. Takasu, and Y. Takahashi, Tools for quantum simulation with ultracold atoms in optical lattices, *Nat. Rev. Phys.* 2(8), 411 (2020)